J Civil Struct Health Monit (2016) 6:619–636
DOI 10.1007/s13349-016-0180-9

ORIGINAL PAPER

Infrared thermography for civil structural assessment: demonstrations with laboratory and field studies

Shuhei Hiasa[1,2] · Recep Birgul[3,4] · F. Necati Catbas[1]

Received: 4 March 2016 / Revised: 27 May 2016 / Accepted: 27 May 2016 / Published online: 13 June 2016

Abstract A detailed investigation of infrared thermography (IRT) for civil structures is presented by considering different technologies, data analysis methods and experimental conditions in the laboratory and also in the field. Three different types of infrared (IR) camera were compared under active IRT conditions in the laboratory to examine the effect of photography angle on IRT along with the specifications of cameras. It is found that when IR images are taken from a certain angle, each camera shows different temperature readings. However, since each IR camera can capture temperature differences between sound and delaminated areas, they have a potential to detect delaminated area under a given condition in spite of camera specifications even when they are utilized from a certain angle. Furthermore, a more objective data analysis method than just comparing IR images was explored to assess IR data, and it is much easier to detect delamination than raw IR images. Specially designed laboratory and field studies show the capabilities, opportunities and challenges of implementing IRT for civil structures.

Keywords Infrared thermography · Non-Destructive Evaluation · IR photography angle · Bridge deck inspection · IR data processing

✉ F. Necati Catbas
catbas@ucf.edu

Shuhei Hiasa
hiasa615@Knights.ucf.edu; s.hiasa.aa@w-nexco.co.jp

Recep Birgul
rbirgul@gmail.com

[1] Department of Civil, Environmental, and Construction Engineering, University of Central Florida, 12800 Pegasus Drive, Suite 211, Orlando, FL, USA

[2] West Nippon Expressway Company Limited (NEXCO-West), Dojima Avanza 19F, 1-6-20 Dojima, Kita-ku, Osaka 530-0003, Japan

[3] Present Address: Mugla Sitki Kocman University, Muğla, Turkey

[4] Formerly, Visiting Scholar at the University of Central Florida, 12800 Pegasus Drive, Suite 211, Orlando, FL, USA

1 Introduction

1.1 Background

The infrared thermography (IRT) is a Non-Destructive Evaluation (NDE) method, and has been developed to detect existing subsurface deteriorations including delaminations and voids in concrete. Traditionally, bridges have been inspected by hammer sounding and/or chain drag, and visual inspections by qualified engineers and inspectors; however, these methods require a lot of field labor and lane closures, especially for bridge deck inspections. IRT offers inspectors the advantage of being able to identify such invisible deteriorations as delaminations and inner voids with reasonable accuracy; it also helps avoid the time and expense of gaining immediate access to the concrete surface to conduct traditional sounding tests. In Japan, IRT application is recommended as a precursor to pinpoint possible presence of defects for further and detailed inspections by traditional methods such as hammer sounding [1]. By incorporating IRT to the concrete inspection process, inspectors can focus their hammer sounding test activities on those areas provided by IRT as likely to be defective. Furthermore, in the USA, IRT has been applied for bridge deck inspections from a traveling vehicle at a normal driving speed for several years in

combination with a high-definition digital image system, although the ASTM standard recommends a value of less than 16 km/h (10 mph) for data collection speed [2]. The combination of IRT and computer vision-based techniques has the potential to replace or reduce the applications of traditional bridge inspection methods since both techniques allow for non-contact applications in a more efficient and effective manner. Using IRT and computer vision-based techniques, data can be collected from a vehicle traveling at a normal speed without any lane closures that are mostly required by traditional methods and other NDE techniques.

Although much research on IRT has been conducted up to the present, most of the studies were conducted under different conditions, making it difficult to draw generalized conclusions. Therefore, there are still several uncertainties regarding the accuracy and reliability of IRT for application to bridge inspection when compared to the sounding test. Through literature reviews, several factors that might affect the performance of IRT can be excerpted such as data collection time, delamination size, data collection speed, and IR camera specifications.

1.2 Literature review

Regarding data collection time, there are several recommendations; Washer et al. proposed 5–9 h after sunrise to detect subsurface delamination for the solar loading part depending on the defect locations, 51 mm (2 in.) to 127 mm (4 in.) deep delaminations [3, 4], while Gucunski et al. [5] reported that a thermal image recorded 40 min after sunrise yielded a much clearer image than another one recorded around noon. Furthermore, the responses of delaminations were described as weaker in IR images as the time approached 3 P.M. [6]. Kee et al. [7] reported that no indication was found from the IR image taken 3 h and 45 min after sunrise (with the shallowest delamination located at 6.35 cm depth) while the best results were achieved using the cooling cycle in which even 15.24 cm deep delamination could be detected. Watase et al. [8] proposed favorable time windows for inspections depending on the parts of a bridge; noon time for the deck top, and midnight for the deck soffit.

Some researchers have included the effect of delamination size on its detectability using IRT [6, 9–11]; however, each researcher has devised artificial defects of different sizes and, in turn, reported different detectable defect depths. Farrag et al. [12] investigated a relationship between the radius (R: shortest dimension) and the depth of defect surface (d) on the detectability of IRT. They concluded that delaminations and voids with an R/d ratio above approximately 0.45 were detectable up to a depth of 10 cm by IRT.

In terms of data collection speed, while ASTM suggests data collection at a speed of less than 16 km/h (10 mph) [2], Hiasa et al. [13] concluded that when data were collected even at 48 km/h (30 mph), a cooled type detector camera was never affected by data collection speed; on the other hand, uncooled cameras were clearly affected. Hiasa et al. [14] also compared IRT at a normal traveling speed, 64 km/h (40 mph), to other NDE methods that collected data under static conditions at an in-service bridge. The results revealed that a cooled camera showed similar or better performance compared to other NDEs including chain drag, while uncooled cameras indicated a lot of false positive misdetections. From these comparisons, it can be concluded that the factor most likely to affect high-speed application of IRT is the integration time/time constant of an IR camera; in other words, cooled cameras are ideal devices for bridge deck inspection for high-speed scanning since cooled cameras have much shorter integration time than that of uncooled cameras.

As for IR camera specifications, some researchers have pointed out the effect of spectral range. Nishikawa et al. [15] claimed that the short wavelength (SW) machine is influenced by the reflection of the sun and the contrast of the sunshine and the shade, while the long wavelength (LW) machine is influenced by objects such as the sky and the opposite building. Thus, SW machines tend to be utilized during nighttime, and LW cameras tend to be used during daytime applications [16]. Hashimoto and Akashi [17] also found that cameras with spectral range of more than 8 μm were affected by the reflection of the sky, and the effect was getting larger when the angle between IR cameras and the concrete surface became shallower. They took IR images of a bridge substructure using three IR cameras with different types of detectors, Indium Antimonide (InSb 1.5–5.1 μm), Quantum Well Infrared Photodetector (QWIP 8–9 μm), and μ-bolometer (8–14 μm), with 45° of angle from the ground. QWIP and μ-bolometer indicated much lower temperature at some areas of the pier than the surroundings, and those were considered as the reflected temperature of the sky.

2 Research objective

The objective of this study is to explore effects

1. Different camera technologies with different detectors, sensitivity, accuracy resolution, etc.
2. IR image collection with different angles which is an unavoidable condition in field applications.
3. Utilization of a more objective data analysis method.
4. Laboratory and field demonstrations in a comparative fashion.

Several NDE techniques such as IRT, Impact Echo (IE) and Ground Penetrating Radar (GPR) have been developed for effective and efficient bridge inspections. Gucunski et al. [5] and Oh et al. [18] compared efficiencies of different NDE methods at an in-service bridge. In their comparative studies, they used several types of hardware for IE and GPR, and obtained different results depending on their devices. However, only one device was utilized for IRT for their study. Therefore, they might have obtained different results if they used several types of IR cameras. A comparative study focusing on the effects of camera specifications is a crucial approach to scrutinize accuracy and reliability issues of IRT; it may also provide important information in regard to such issues as data collection speed and spectral range. Therefore, this study involves a comparative study conducted with three types of IR cameras. In addition, the effect of photography angle on IRT along with the specifications of IR cameras are also investigated since vehicle-mounted IRT usually utilizes IR cameras with certain angles to capture IR images of the whole lane at one time during bridge deck inspections. Therefore, not only the effect of data collection speed, but also the effect of camera angle depending on camera specifications should be evaluated. Hashimoto and Akashi [17] reported the effects of photography angle with different spectral range cameras under passive IRT conditions. This study evaluates the effects of photography angle under active IRT conditions for the laboratory studies but utilizes only ambient conditions, making it more challenging for field studies.

In the present work, a more objective method than just comparing IR images was explored to assess IR data when evaluating the effects of photography angle and camera specifications. Since concrete structures do not always have homogeneous temperatures due to differences of locations and orientations with respect to the sun as discussed by Washer et al. [4], sometimes IRT makes it difficult to interpret the data from raw IR images due to a lot of noise depending on the time of photography as reported in [5]. As Washer et al. [19] argued, if the temperature span for IR images is setup around 2 °C, while some defects can be detected clearly, some anomalies generate higher/lower temperature than the temperature span and IRT cannot detect them at the temperature span. Therefore, they recommended adjusting the temperature span of IRT continuously throughout inspections. However, it might require a lot of work during or after the bridge inspection. Chase et al. [20] developed the time lapse infrared thermography system to detect deeper defects than the normal IRT which detects defects from raw IR images. However, it requires continuous data collection at specific intervals, 20 min in their study, for at least one full day from a fixed location. Therefore, it is still not an efficient methodology for bridge deck inspections since bridge decks are too large to capture whole deck images several times in a day. Kee et al. [7] and Oh et al. [18] were trying to process IR data with thresholds defined by iterative trials in each IR image. Therefore, an easier and more reliable data processing methodology was explored from the results obtained under laboratory and field conditions.

3 IR test setup

3.1 Infrared cameras

In this study, three infrared cameras with different specifications as shown in Table 1 (T420, T640 and SC5600 manufactured by FLIR Systems, Inc.) were utilized to evaluate the differences of camera specifications. As mentioned above, when different types of hardware for IE and GPR were compared, they produced different results. Similarly, IRT must also be compared with different types of IR hardware to accurately evaluate the differences in inspection reliability.

As described in Table 1, T420 and T640 have the same type of detector, uncooled micro bolometer, while SC5600 has an InSb detector. IR cameras can be classified into two types according to their detector type: thermal detectors and quantum detectors, and these are often called uncooled and cooled detectors/cameras, respectively. T420 and T640 are classified as uncooled type, while SC5600 is categorized as a cooled camera. Typically, uncooled cameras have lower costs and a broader spectral response than cooled cameras, although their response is much slower and less sensitive than cooled cameras [21]. In terms of the spectral range, SC5600 captures medium wavelength while others capture long wavelength. Regarding the pixel resolution, SC5600 and T640 have approximately the same imaging resolution, and their resolutions are 4 times higher than T420. Moreover, they have different thermal sensitivities; SC5600 is the most sensitive IR device, then comes T640 which is more sensitive than T420 as shown in Table 1. Therefore, the effects of spectral range, thermal sensitivity, and resolution are compared in this study. As for the integration time (time constant), since this comparative study is conducted under static conditions, the effect of the differences of integration time is negligible.

3.2 Settings of test specimens

In this laboratory test, three types of separate concrete test pieces as displayed in Fig. 1 with different thicknesses were attached to a wooden board, 90 × 180 × 1.8 cm in size, as shown in Fig. 2. The board can be heated up using an electric heating mat, which is installed behind the

Table 1 Three infrared cameras used in this study and their primary specifications

Camera number	T420	T640	SC5600
Detector type	Uncooled microbolometer	Uncooled microbolometer	InSb
Thermal sensitivity (NETD)	<0.045° at 30 °C	<0.035 °C at 30 °C	<0.02 °C at 25 °C
Accuracy	±2 °C or ±2 %	±2 °C or ±2 %	±1 °C or ±1 %
Resolution (pixels)	320 × 240	640 × 480	640 × 512
Spectral range (μm)	7.5–13	7.5–14	2.5–5.1
Frame rate (Hz)	60	30	100
Field of view	25° × 19°	25° × 19°	20° × 16°
Integration time/time constant (electronic sutter speed)	12 ms	8 ms	10 μs–20 ms

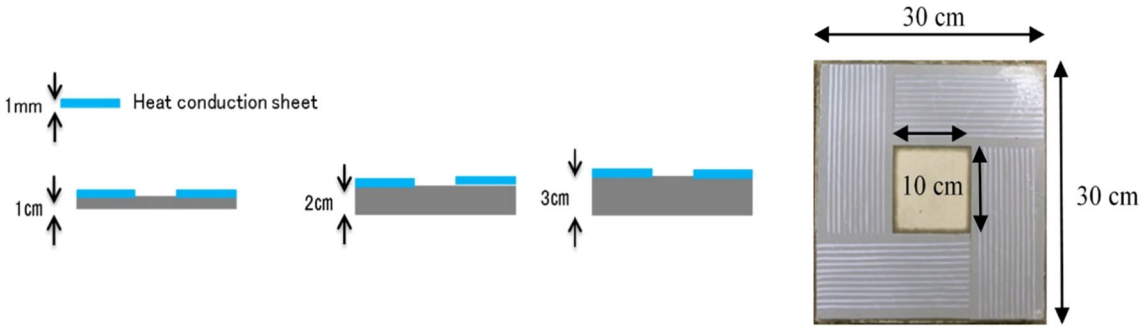

Fig. 1 Test pieces ($t = 1$ cm, $t = 2$ cm, $t = 3$ cm)

Fig. 2 Test plates attached to the wooden board

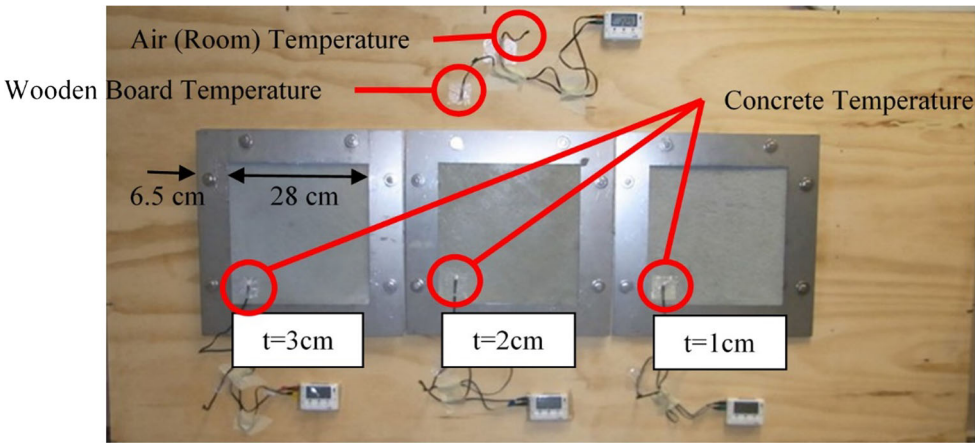

wooden board as shown in Fig. 3. The room's ambient temperature and surface temperatures of the wooden board and test specimens were recorded by thermocouples as presented in Fig. 2. The concrete test pieces were manufactured and used to simulate artificial delaminations at the middle part. As described in Fig. 4, the space between the actual test piece and the wooden board is achieved by attaching a 1 mm thick heat conduction sheet, which simulates an artificial delaminated area. Since the part of the test piece attached to the heat conduction sheet can exchange heat with the wooden board, that part represents the sound area of the concrete surface. On the other hand, air present in the space at the center prevents heat exchange with the wooden board; thus, that part represents the delaminated area and generates temperature contrast between the middle part and its perimeter areas.

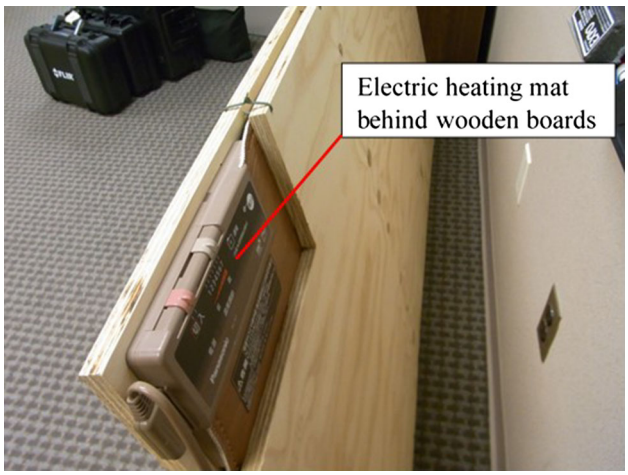

Fig. 3 Electrically heating mat behind wooden boards

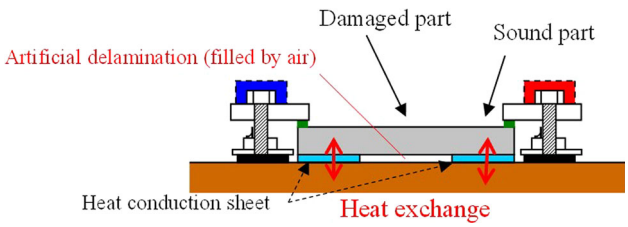

Fig. 4 Structure of test piece

3.3 Photography methods and temperature conditions

Infrared images were taken from a distance of 5.0 m by the three different IR cameras at the same time with angles of 0°, 30° and 45° (where 0° is perpendicular). Photography of each angle case was conducted at different days to keep a steady state in the temperature of test specimens at the beginning of heating. The photographing cases are as follows;

Case 1 Photographing angle = 0° (Fig. 5)
Case 2 Photographing angle = 30° (Fig. 6)
Case 3 Photographing angle = 45° (Fig. 7)

In this laboratory test, the heat source for the test pieces was an electric heating mat only, which was set up between wooden boards on which test specimens are attached. Since this test was conducted indoors, the room temperature was almost stable due to the use of air conditioning in the room. During the experiment, each temperature was measured by thermocouples as exhibited in Fig. 2, and temperature records are also drawn in Figs. 5, 6 and 7. As can be seen, each sound concrete temperature goes up gradually as the wooden board is warmed by the heat mat while the room temperature is almost stable. Furthermore, it is also obvious that a thinner concrete specimen is warmed up faster than a thicker specimen. This means that heat was transmitted from the backside of the concrete plates to their front side since there is no other heat source except the wooden board, and the speed of heat propagation depends on the thickness. From these results in each case, it was verified that the sound part of each test specimen could successfully exchange heat with the wooden board through the heat conductive sheet. However, these temperatures were lower than the temperatures captured by IR cameras. A possible explanation for this behavior is that thermocouples used in this experiment registered temperature values that are a combination of both concrete surfaces and the room temperature which happens to be the lowest temperature in the testing environment. Therefore, this combination gives rise to a lower temperature reading on a concrete surface than the actual temperature value of the surface. On the other hand, IR devices continuously register temperature values of the concrete surfaces. Hence, results from thermocouples were only used for verification of heat exchange between concrete plates and the wooden board.

Furthermore, to validate whether the wooden board was heated up uniformly by the electric heating mat, IR images taken by SC5600 were investigated. Figure 8 displays some of them taken at 0, 15, 30 and 75 min after turning the heating mat on. It can be observed that the wooden board was heated up evenly except the edge part. Furthermore, Fig. 9 depicts four points of temperature around test specimens as shown in left upper image of Fig. 8 at every 5 min. It is obvious that each temperature is increasing at the same rate. Therefore, it can be concluded that the wooden board was heated up uniformly by the electric heating mat under the given conditions.

4 Test results

4.1 Comparison of temperature readings from infrared cameras

To investigate the effect of photography angle depending on camera specifications on IRT for delamination detection, temperature readings from IR cameras were compared. In this comparison, two points, delaminated and sound areas, of temperatures as indicated in Fig. 10 were read from each IR image. Figures 11, 12 and 13 gives temperatures of each point for each thick test specimen in each case. When comparing the three graphs, each camera of Case 1 indicates closer temperature readings at each time compared to Cases 2 and 3, although T640 indicates a little higher temperature than the other 2 cameras, even in Case 1. On the other hand, in Cases 2 and 3, every camera displays different temperatures approximately 0.5–3 °C,

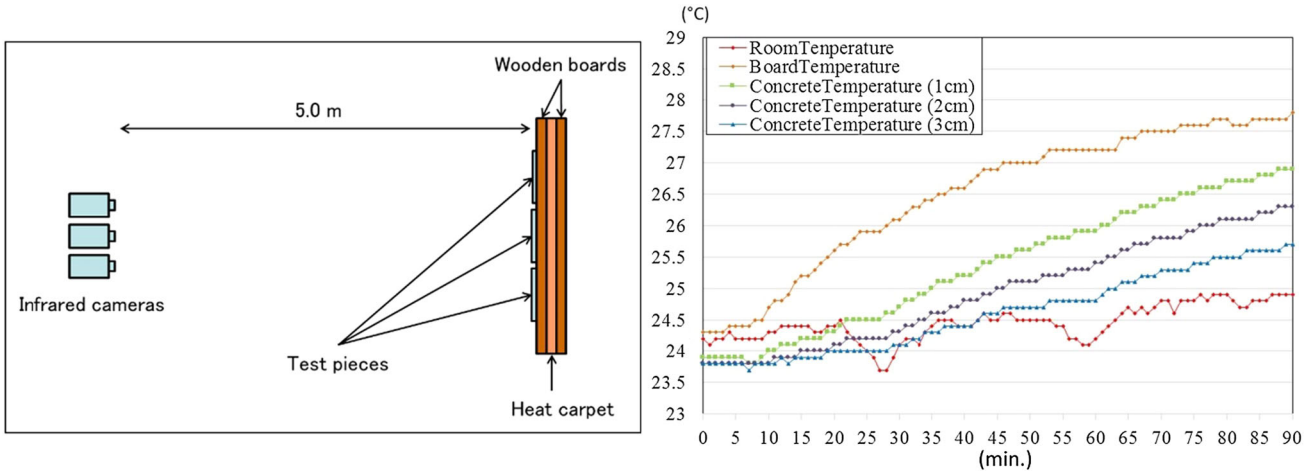

Fig. 5 Photography situation of Case 1 (*left*) and the temperature records (*right*)

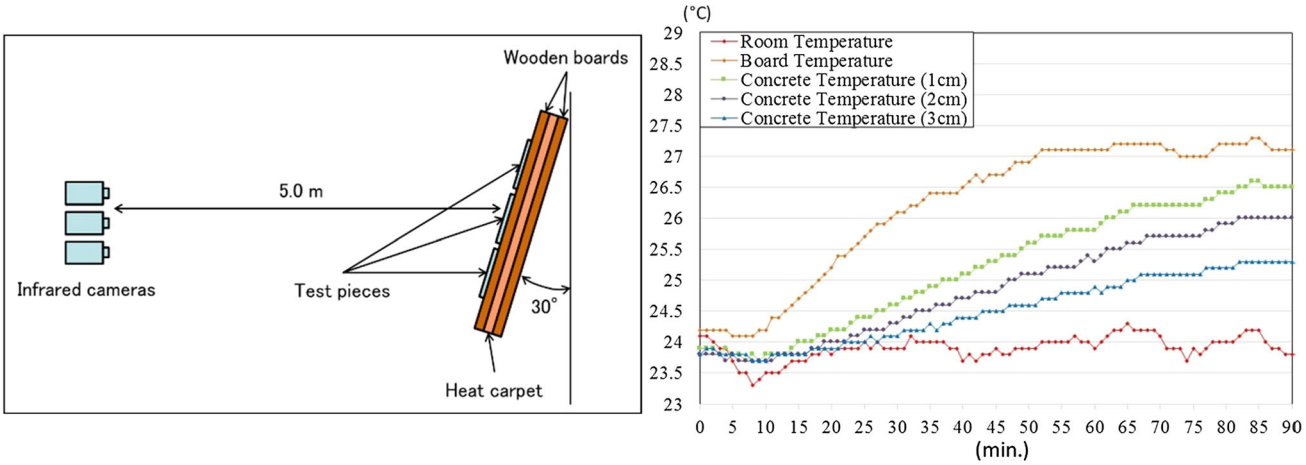

Fig. 6 Photography situation of Case 2 (*left*) and the temperature records (*right*)

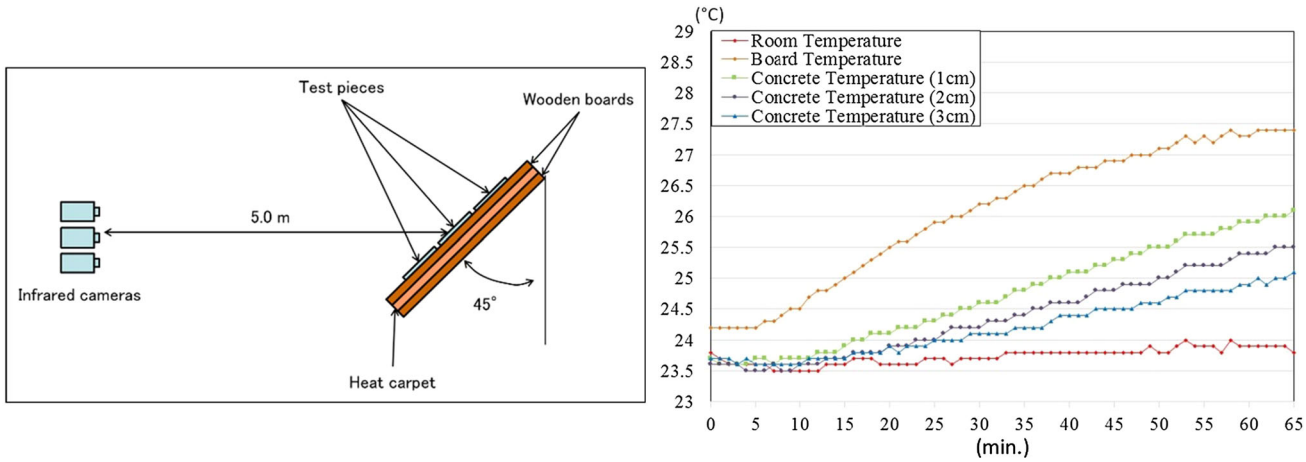

Fig. 7 Photography situation of Case 3 (*left*) and the temperature records (*right*)

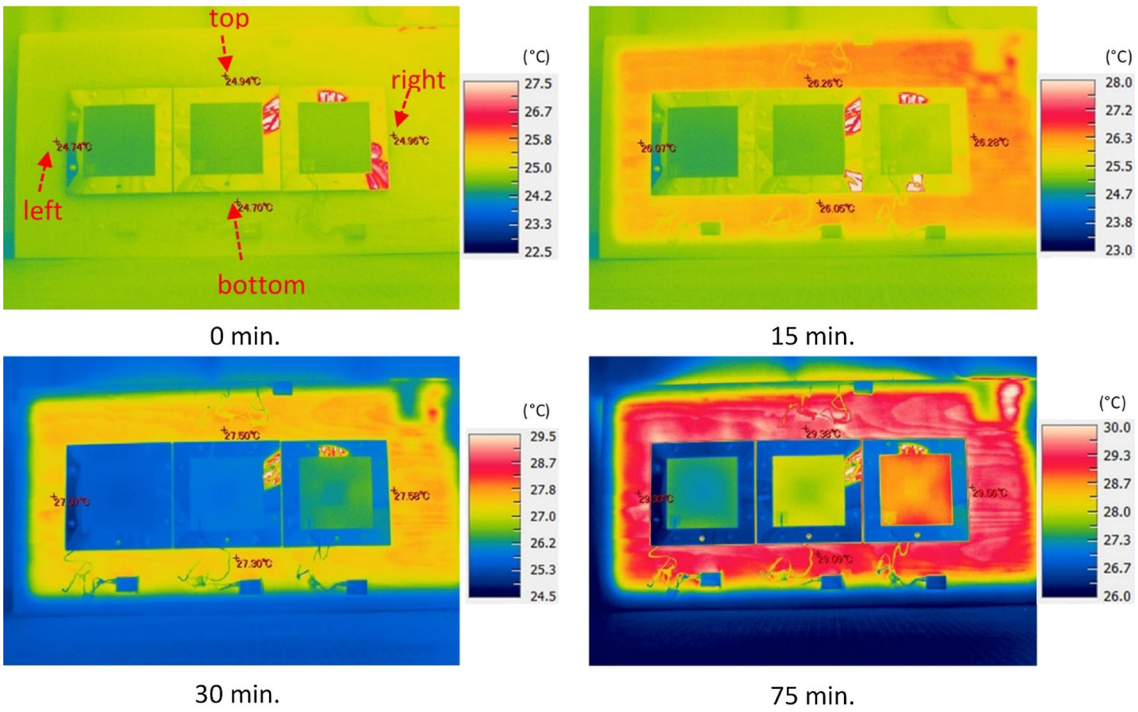

Fig. 8 IR images taken by SC5600 at each time

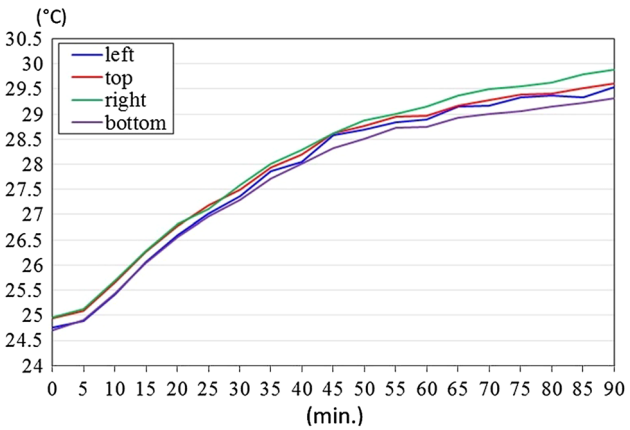

Fig. 9 Temperature readings at each point at each time

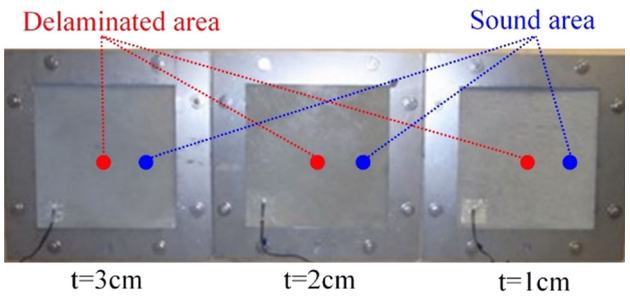

Fig. 10 Points for temperature comparison by infrared readings

even though each temperature rises at a similar rate. These differences might be caused by the reflection of an object on the angle of reflection for LW cameras, T640 and T420, as argued in [15]. Furthermore, temperature readings of SC5600 dropped after 25 min in Case 2, and 15 and 40 min later in Case 3 about 1 °C. This can be considered that the air conditioner of the room worked at that time, and test pieces were blown directly or indirectly due to convection. In terms of Case 1, the wooden board and specimens might be set up in parallel to the direction of the wind, and might not be influenced by air convection. Here, the air conditioner system was set up to start working when the room temperature became more than a certain temperature. However, both T640 and T420 do not show the change in both Cases 2 and 3, and the possibility of influence of refraction by an object can be considered. Even though the absolute value of each IR camera in each case is different, temperature differences between delaminated and sound areas can be seen from each camera in each case regardless of different temperature readings from other cameras.

Capturing accurate temperature is important, however, detecting thermal contrast between sound and delaminated areas is the most important thing for IRT to detect delaminated areas from concrete structures since the detectability of IRT is grounded on the temperature difference. The mechanism of IRT is that if there is an interior delamination of a concrete structure, that part is filled by air and the air

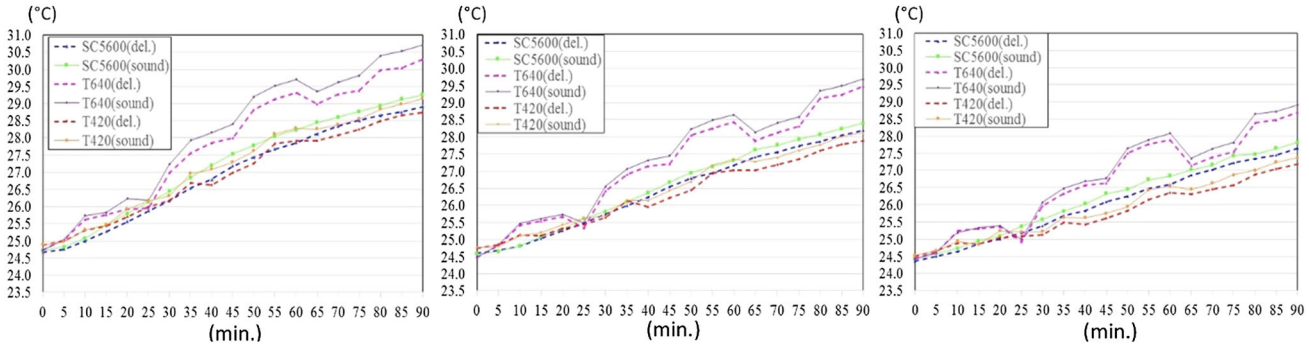

Fig. 11 IR readings (Case 1: Photographing angle = 0°, *left* 1 cm, *middle* 2 cm, *right* 3 cm)

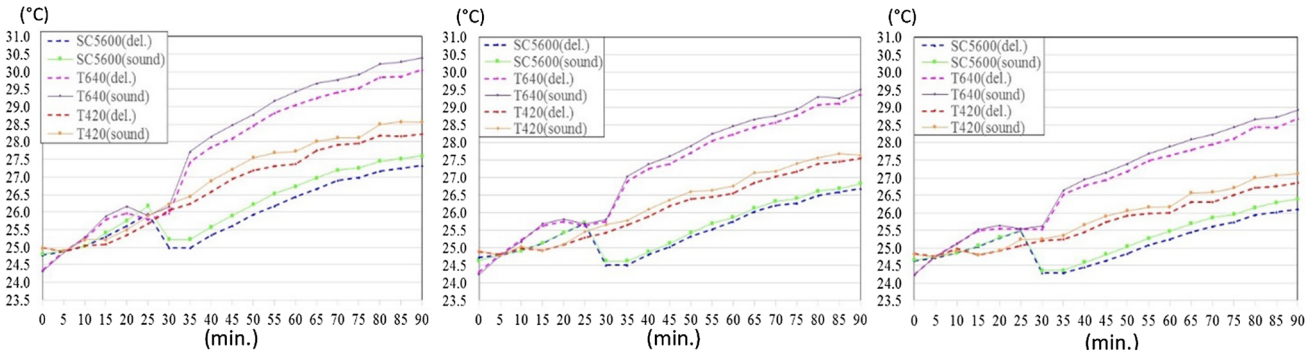

Fig. 12 IR readings (Case 2: Photographing angle = 30°, *left* 1 cm, *middle* 2 cm, *right* 3 cm)

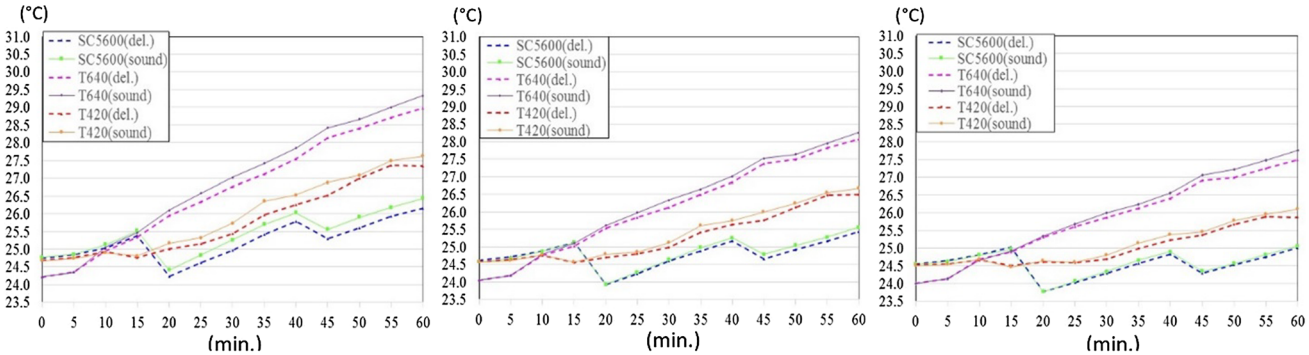

Fig. 13 IR readings (Case 3: Photographing angle = 45°, *left* 1 cm, *middle* 2 cm, *right* 3 cm)

acts as a thermal insulator (thermal conductivity of air 0.0241 W/m °C) and prevents heat from penetrating to the concrete (thermal conductivity of concrete 1.6 W/m °C) beneath the delamination. Thus, the concrete above the delamination yields different temperature compared to the surroundings depending on ambient temperature [22]. IRT detect interior defects by capturing those temperature differences of concrete surface by reading the emitted electromagnetic radiation from the concrete surface and converting it to temperature [23]. Therefore, temperature differences between 2 points were summarized Figs. 14, 15 and 16 (minus means delaminated area is cooler than sound area). The graphs on the left describe thermal contrast for each specimen in Case 1, middle ones are Case 2 and the graphs on the right show Case 3. Even though the measurement time periods are different, each camera in each case describes a similar result; 1 cm thick specimen made the highest temperature difference while 2 and 3 cm thick specimens yielded almost the same thermal contrast between the two points in this laboratory test. Furthermore, every delaminated area in each case indicates cooler temperature than the surrounding sound area after 20–30 min of turning on the electric heating mat; hence, these delaminations should be detected by IRT.

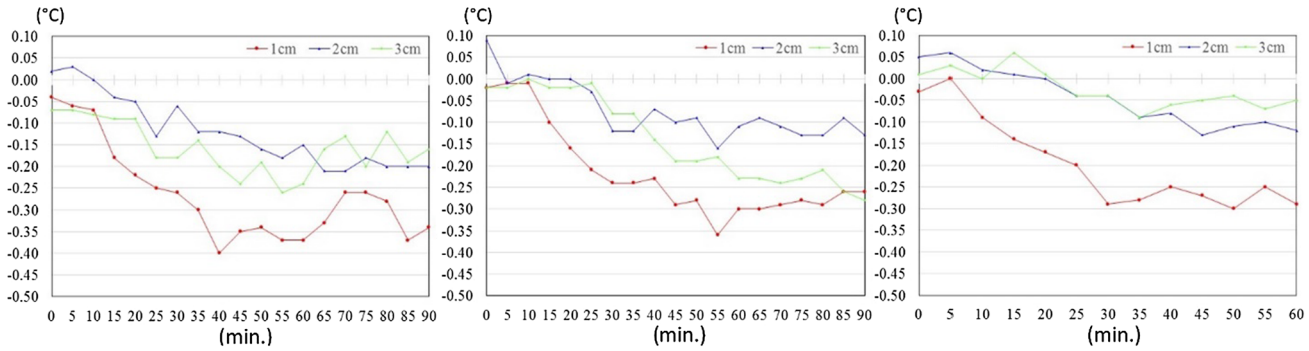

Fig. 14 Temperature difference of SC5600 (*left* Case 1, *middle* Case 2, *right* Case 3)

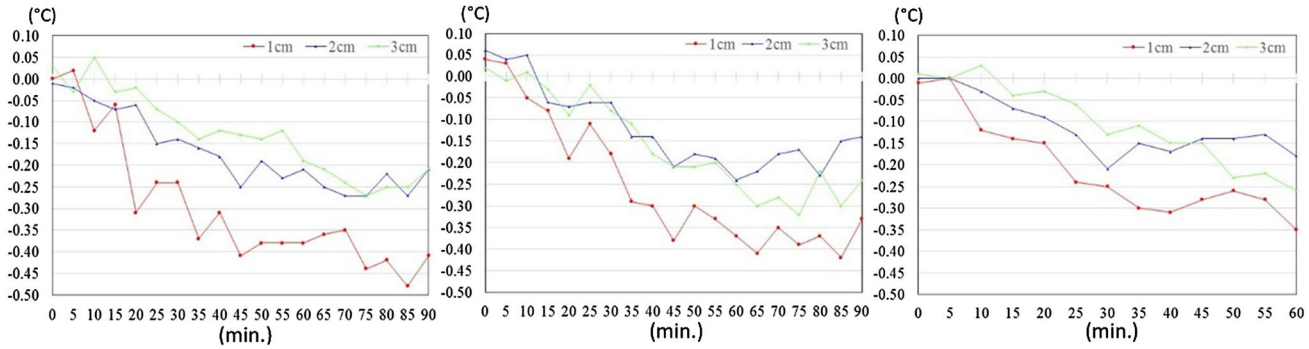

Fig. 15 Temperature difference of T640 (*left* Case 1, *middle* Case 2, *right* Case 3)

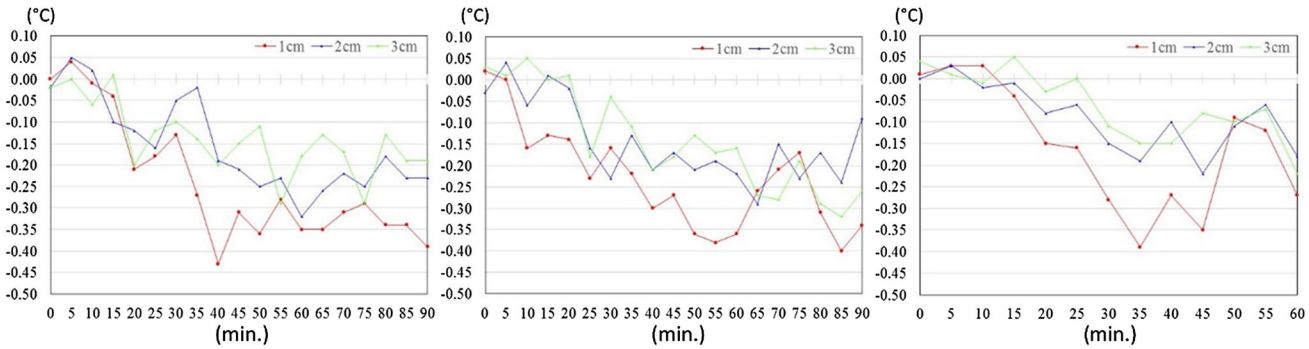

Fig. 16 Temperature difference of T420 (*left* Case 1, *middle* Case 2, *right* Case 3)

In conclusion, when IR images are taken at a perpendicular angle from the objects, IRT is less sensitive than when it is taken from a certain angle regarding temperature reading of different types of IR cameras. However, even different IR cameras capture different temperatures from the concrete surface when they are utilized at a certain angle, they have a potential to detect a delaminated area under a given condition in spite of different camera specifications since each IR camera can capture temperature differences between sound and delaminated areas.

4.2 Comparison of IR images

One of the valuable advantages of IRT is the easiness of wide range concrete surface scanning based on IR images, which indicate delaminated areas by different colors. In the comparison of IR readings, it was found that each camera was able to capture temperature differences between sound and delaminated areas. Therefore, the visibility of delamination detection from each IR image was compared, and an investigation was conducted on how a difference in camera specifications and photography angle affect the

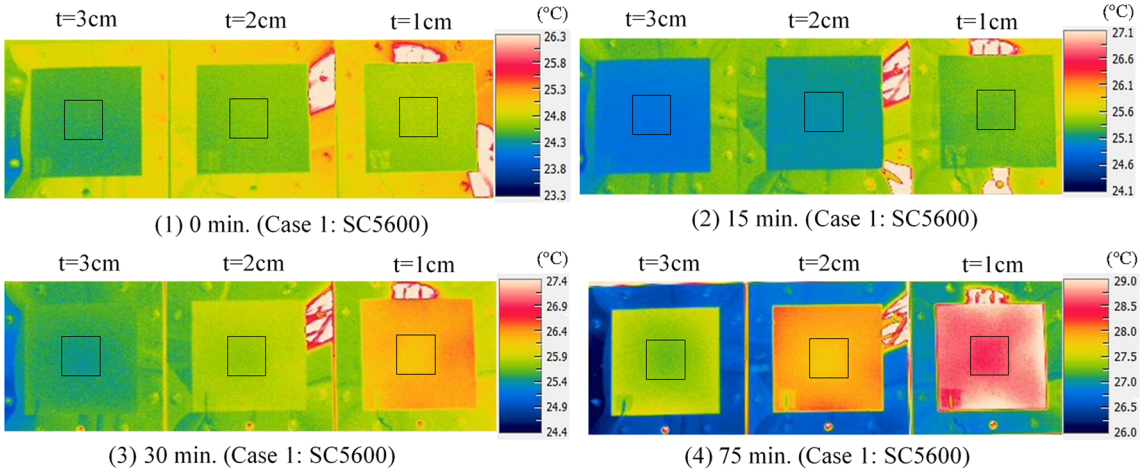

Fig. 17 Raw IR images taken at several times by SC5600 (Case 1)

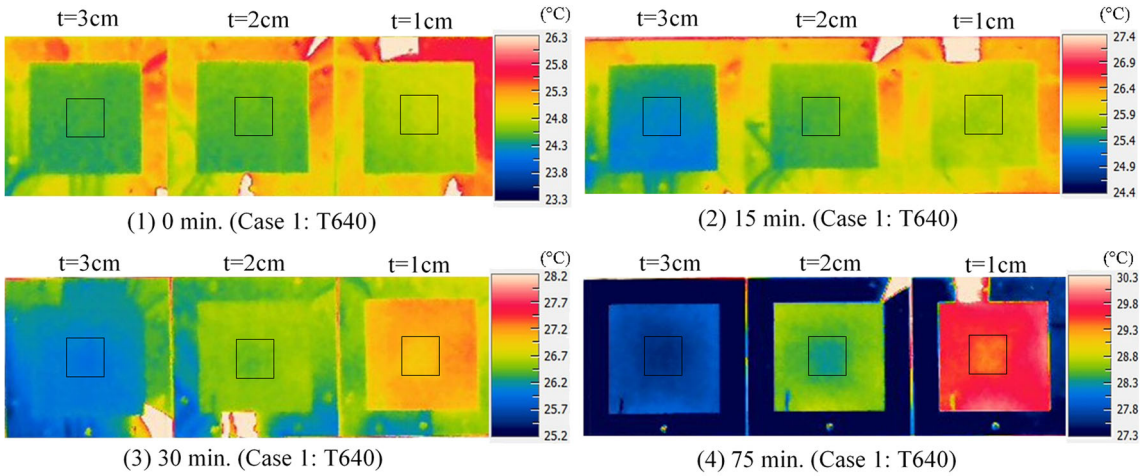

Fig. 18 Raw IR images taken at several times by T640 (Case 1)

visibility of damage detection in this section. Figures 17, 18 and 19 show IR images taken by each camera in Case 1, respectively at several times: (1) 0 min after turning the heating mat on, (2) 15 min after turning the heating mat on, (3) 30 min after turning the heating mat on, (4) 75 min after turning the heating mat on. In these images, concrete specimens are surrounded by metal frames as displayed in Fig. 2 to stick concrete pieces on the wooden board without any voids between the wooden board and heat conduction sheets. Therefore, those parts were ignored in the evaluation since metal frames reflect temperatures of frontal objects like mirrors. Furthermore, delaminated areas are enclosed by dotted line. The temperature range of the IR images was set up to 3.0 K for all images as Washer et al. suggested in [19], and the level setting was adjusted manually for each IR image to figure out the color contrast between the middle and surrounding areas.

As can be seen in (1) of each Figs. 17, 18 and 19, surface temperatures of each concrete test piece were stable when the test got started, and any damage indication was not found from any camera. After 15 min elapsed as displayed in (2), a slightly square shape appeared in the IR image of 1 cm thick test specimen taken by SC5600. Similarly, the change of color at the middle point for 1 cm thick concrete plate can be seen from the image taken by T640, although the indication and the shape are more obscure than SC5600. In terms of T420, no indication can be recognized after 15 min. Then, after 30 min have passed as can be seen in (3), SC5600 shows color contrast at the middle area of each test piece, while T640 and T420 indicate contrast for 1 and 2 cm thick specimens, even though some of them are not clearly visible. At the point of 75 min later, every camera displays color contrast on all test specimens at the middle areas, even though the shapes are not exactly square especially when the plate is getting thicker.

In case of photography with a certain angle, Fig. 20 shows results of Case 2, Photographing angle = 30°, at the

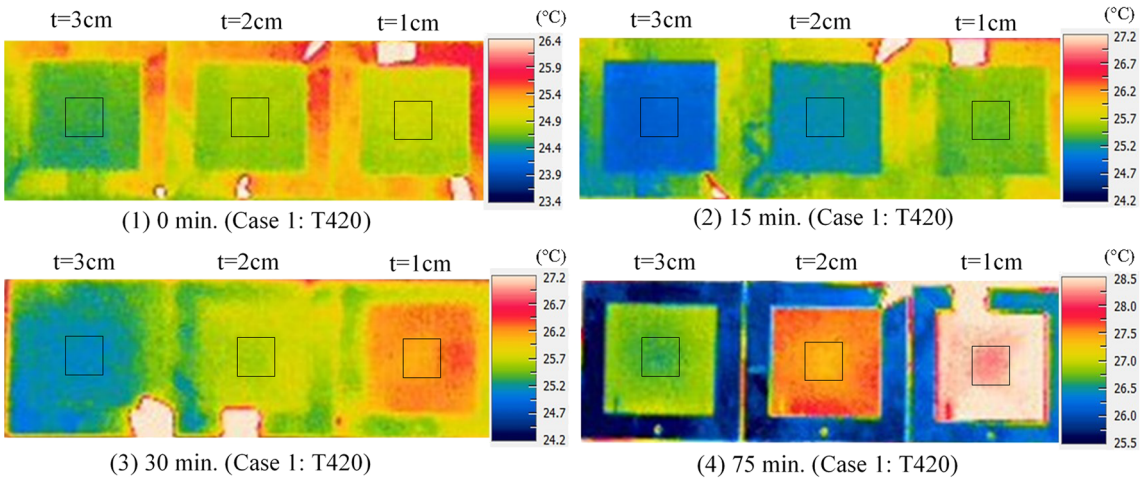

Fig. 19 Raw IR images taken at several times by T420 (Case 1)

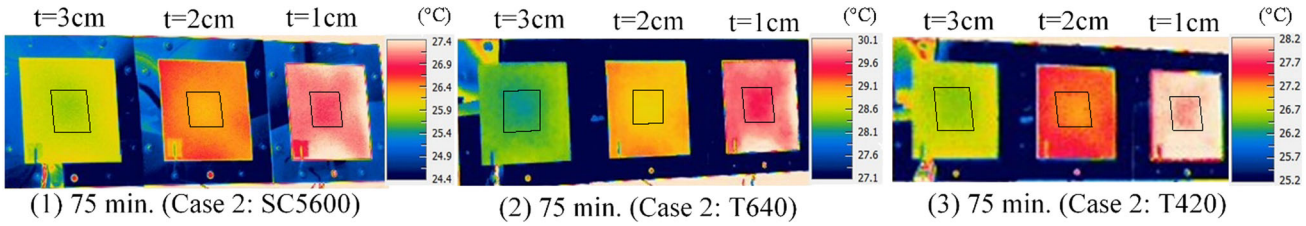

Fig. 20 Raw IR images taken by each camera at 75 min after heating started (Case 2)

point of 75 min later and Fig. 21 displays IR images of Case 3, Photographing angle = 45° after 60 min have passed. In both cases, color contrast can be recognized at the middle areas of each test specimen by any IR cameras. In these cases, the shapes are getting obscure for thicker specimens. Regarding the effect of camera specifications for delamination detection by IRT, no big difference can be recognized from the comparison of IR images taken at these laboratory tests since each delaminated part was detected by every camera after the elapse of a certain time. However, SC5600 depicts indications most clearly among these three cameras in any cases and times, and SC5600 and T640 yielded color contrast between delaminated and sound areas faster than T420. These results indicate that thermal sensitivity/accuracy and resolution might affect IRT results regarding the visibility of damage indication.

5 Processing IR data

5.1 Methodology of data processing

One of the challenges of IRT is how to interpret and detect delaminations from IR images since it becomes very subjective to judge whether the color contrast of the image is a damage indication or not. Actually, since it was known that there was a delaminated area at the middle part of each specimen, the temperature span setting was focused on whether the middle part showed color contrast. As can be seen in Sect. 4.2, when the temperature difference between sound and delaminated parts is very small, less than 0.5 °C in this experiment, the color contrast of IR images becomes unclear, and it would lead to different judgments depending on the person. Furthermore, it is not always possible to detect subsurface delaminations in concrete structures under a natural environment, namely passive IRT condition, only from the color variation of raw infrared imagery since the concrete structure itself tends to have a temperature gradient depending on location and orientation with respect to the sun as discussed by Washer et al. [4]. Therefore, a more objective data processing method was explored using MATLAB in this study. Since every IR image consists of a group of pixels, and each pixel has a numerical value, IR data can be manipulated mathematically. The left image of Fig. 22 displays a scaled version of the original IR data after 75 min in Case 1 (Angle = 0°) by SC5600. However, it is difficult to distinguish a delaminated area from this image. Therefore, the left image of Fig. 22 is specified a range of gray levels, such that all values lower than the delaminated area are depicted as

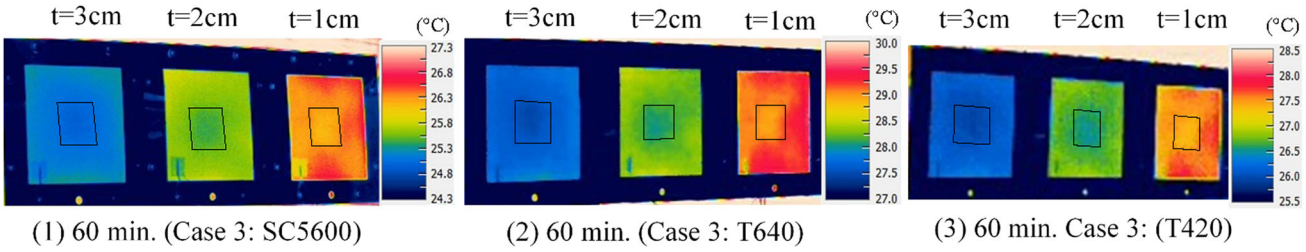

Fig. 21 Raw IR images taken by each camera at 60 min after heating started (Case 3)

Fig. 22 Scaled IR data (**a**) and specified range of IR data (**b**)

black ("0" in MATLAB) and all values greater than the sound area are drawn as white ("1" in MATLAB), where both temperatures are values of two points described in Fig. 10, and all intermediate values are scaled within the range as given in Eq. (1)

$$\mathrm{F}(x,y) = \begin{cases} 0 & (if\ T(x,y) \le T(\mathrm{del.})) \\ 1 & (if\ T(x,y) \ge T(\mathrm{sound})) \\ \dfrac{T(x,y) - T(\mathrm{del.})}{T(\mathrm{sound}) - T(\mathrm{del.})} & (if\ T(\mathrm{del.}) < T(x,y) < T(\mathrm{sound})) \end{cases} \quad (1)$$

where $T(x, y)$ is the temperature value of each pixel, T(del.) is the temperature of delaminated part, T(sound) is the temperature of sound area and $F(x, y)$ is the specified value of each element. The right image of Fig. 22 is the result, and it provides a much more clear indication at the middle part of the image than the IR image displayed in Fig. 17. Here, the surrounding black flame is made by a metal frame and the black square shape at the lower left is yielded by a thermocouple and the tape to attach it onto the test specimen; hence, those are ignored from the judgment. Yet, there is still a lot of noise on the sound area. This means that even in laboratory test conditions, the concrete surface temperature of the sound area never becomes homogeneous. However, it can be assumed that the temperature of the sound area must be much closer to the temperature of the sound area than the delaminated area. Figure 23 depicts a schematic image of the temperature gradient of the surface. Assuming that the temperature of the sound area is constant and the center of the delaminated area is the lowest temperature on the concrete surface, it can be

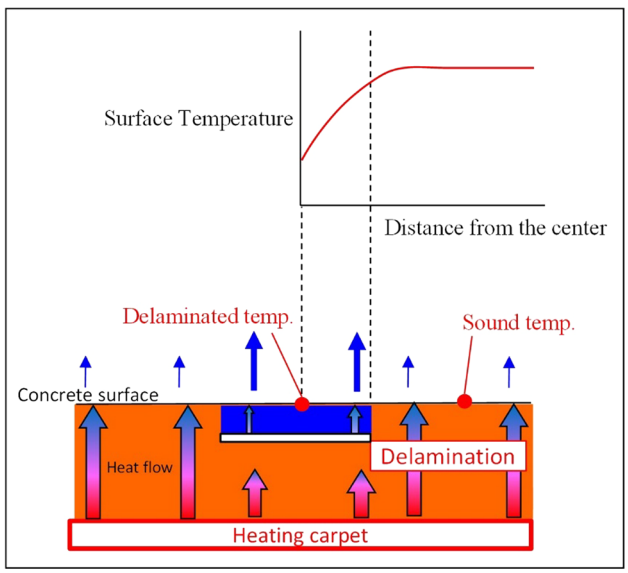

Fig. 23 Image of surface temperature of test specimens

concluded that the temperature of the delaminated area increases gradually as it approaches the edge of the delamination and the temperature becomes constant at a point of the sound part near the delaminated area. Therefore, if those temperatures close to the sound area are removed, much of the noise should be erased. Figure 24 shows a binary image of each case that only the bottom 10–50 % of the specified range displays as black ("0" in MATLAB) and the others are drawn as white ("1" in MATLAB) as shown in Eq. (2).

Fig. 24 Binary images (Case 1: SC5600, 75 min.)

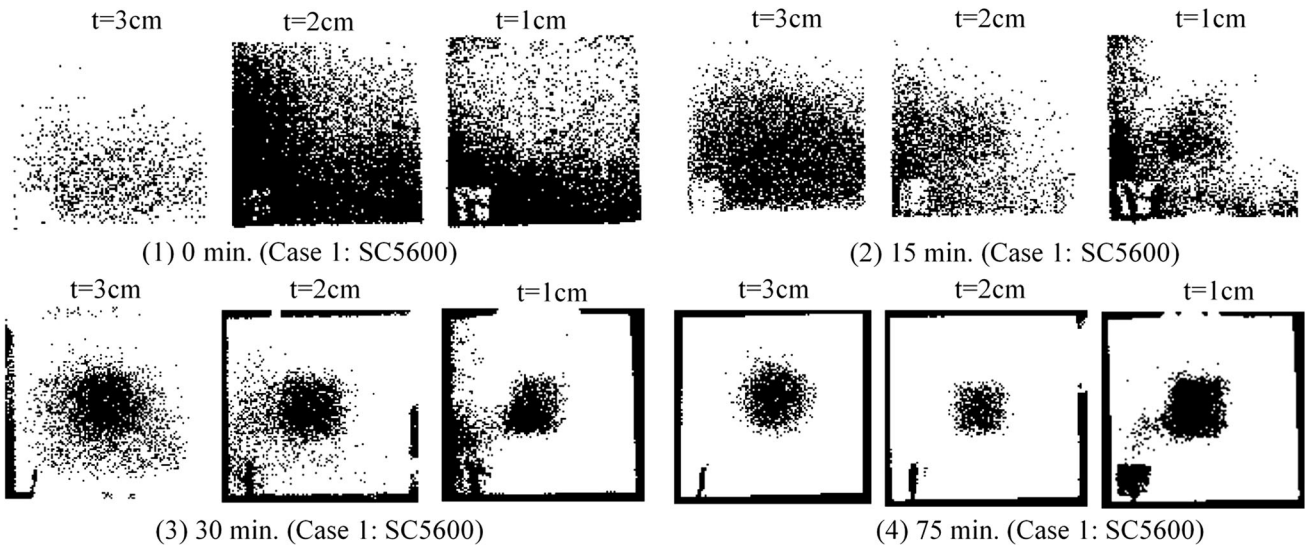

Fig. 25 Processed IR images taken at several times by SC5600 (Case 1)

$$G(x,y) = \begin{cases} 0 & (if\ F(x,y) \leq 0.1 \text{ to } 0.5) \\ 1 & (\text{others}) \end{cases} \quad (2)$$

where $G(x, y)$ is the value of each element of binarized image. Then, from these images, an image, which has relatively less noise and clearer delamination indication is chosen, 20 % was chosen in this case. This procedure is relatively subjective, yet this is a more objective way to judge a delaminated area than it is to decide it from raw IR images since the indication is displayed as black while the sound area is shown as white.

5.2 Comparison of processed images

Based on the methodology described in Sect. 5.1, each IR data shown in Figs. 17, 18, 19, 20 and 21 was processed as displayed in Figs. 25, 26, 27, 28 and 29, respectively. In terms of Case 1, photography angle = 0°, no camera can detect delamination at the beginning of the test as can be seen in (1) of each figure. After 15 min have elapsed, 1 and 2 cm images of SC5600 indicate something like a square shape at the middle parts of the images; however, they also depict a lot of noise at the lower left. Still, SC5600 does not show any indication for 3 cm thick concrete plate at this time. T640 also indicates the sign of delamination at the middle area for 1 cm thick plate, although it also shows misdetection at the lower left. Regarding the other two thicknesses, T640 could not detect the delamination. In terms of T420, no indication can be recognized after 15 min. After 30 min have passed as exhibited in (3), both SC5600 and T640 point out delaminations for every thickness of test specimens with some noise, even though SC5600 draws more likely square shapes for each specimens. On the other hand, T420 depicts something like a square shape at the middle parts of the images of 1 and 2 cm thicknesses: however, it also shows a lot of noise at the left. At the point of 75 min later, every camera indicates delaminations on all test specimens at the middle areas with less noise. At this time, SC5600 also indicates more likely square shapes for each specimen than T640 and T420. When comparing T420 to the other two cameras, indications of T420 are much rougher than the others since

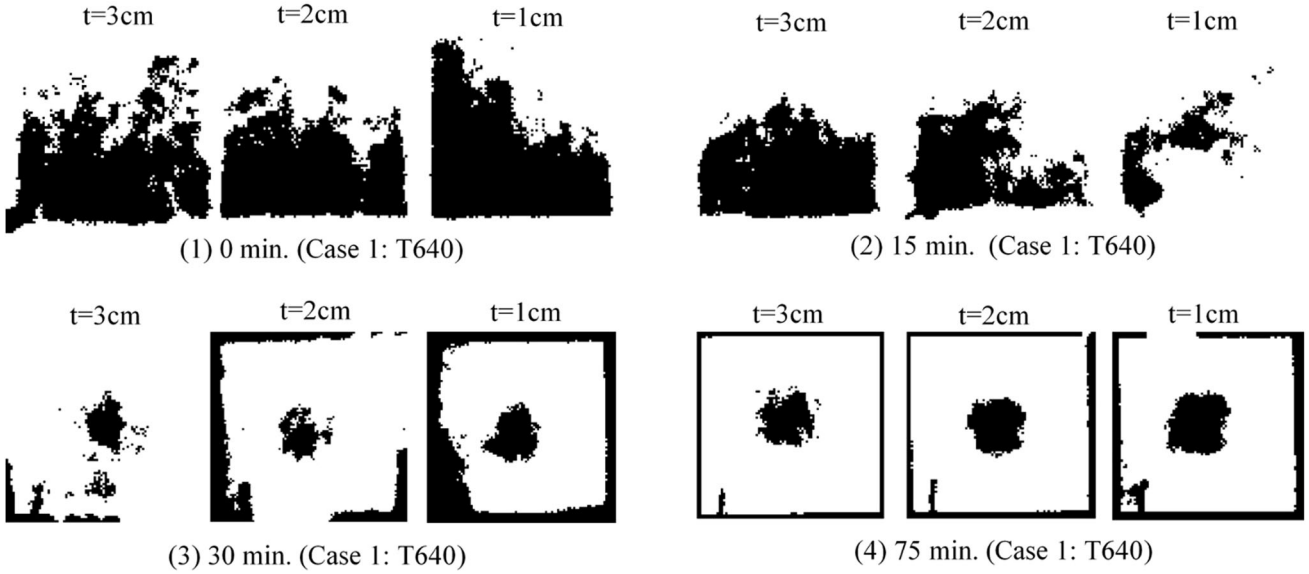

Fig. 26 Processed IR images taken at several times by T640 (Case 1)

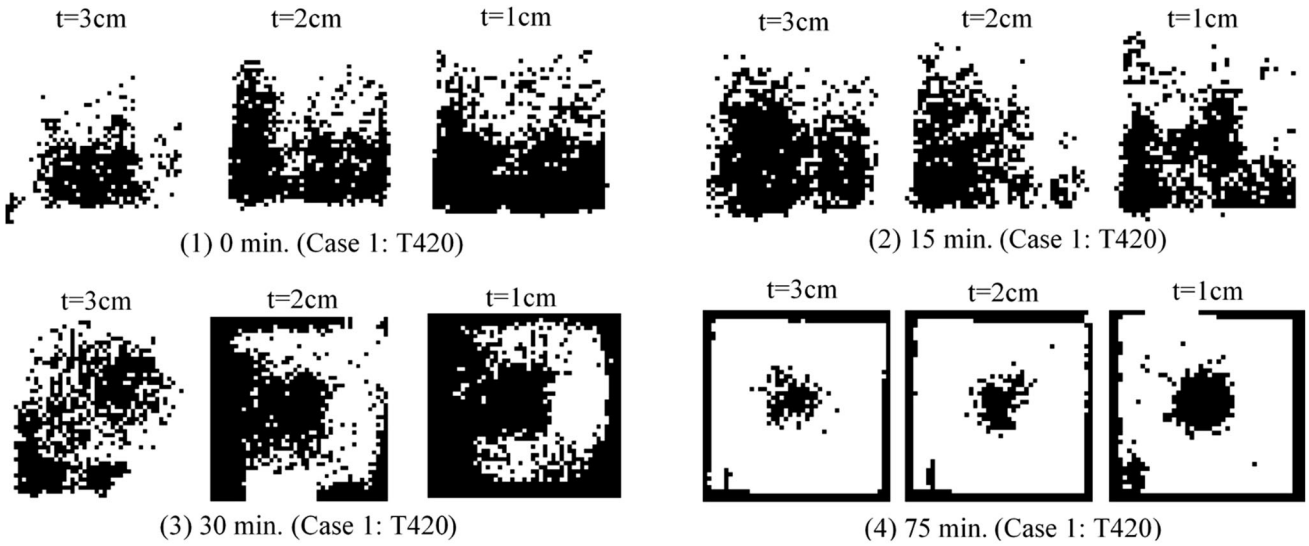

Fig. 27 Processed IR images taken at several times by T420 (Case 1)

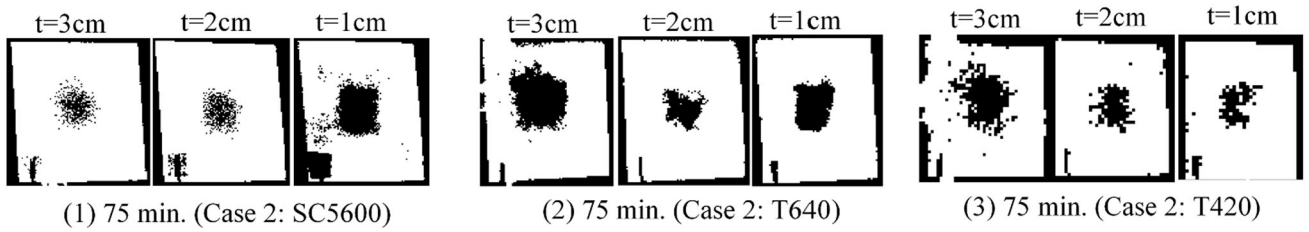

Fig. 28 Processed IR images taken by each camera at 75 min after heating started (Case 2)

the pixel resolution is 4 times smaller than the other cameras, and it might cause lower performance in damage detection for T420.

In regards to photography with certain angles, in both cases, every camera clearly displays delaminations at the middle areas of each concrete plate at the point of 75 min

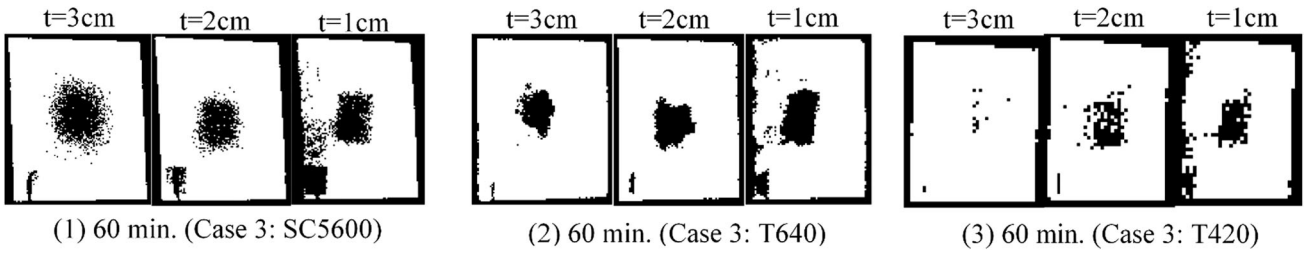

Fig. 29 Processed IR images taken by each camera at 60 min after heating started (Case 3)

Fig. 30 Structure which delamination was found by IRT [*upper* the structure (used to be a water tank), *lower left* before hammering, *lower right* after hammering]

later for Case 2, Photographing angle = 30°, and after the elapse of 60 min for Case 3, Photographing angle = 45°, even though the only indication of T420 for Case 3 for 3 cm thickness is unclear.

Through the comparison of processed images, only T420 shows lower performance than the other two cameras in terms of delamination detection for IRT. Although SC5600 performs more accurately than T640 since it displays closer shapes of delamination in each case, both cameras successfully depict delaminations at the middle areas of all test specimens after a certain time from the beginning of heating during this laboratory test. Based on the result, it is certain that the pixel resolution of the IR camera affects the performance of IRT, 320 × 240 pixels for 5.0 m distance photography in this case. Thermal sensitivity or accuracy also might affect IRT results since SC5600 shows better performance than T640.

6 Application of the data processing methodology for a real concrete structure

In this section, the data processing methodology was applied to examine how it works for a real concrete structure. In this study, a structure at the University of Central Florida as shown in Fig. 30 was chosen to try the methodology since a delamination was already found from the structure by IRT before as reported by Catbas et al.

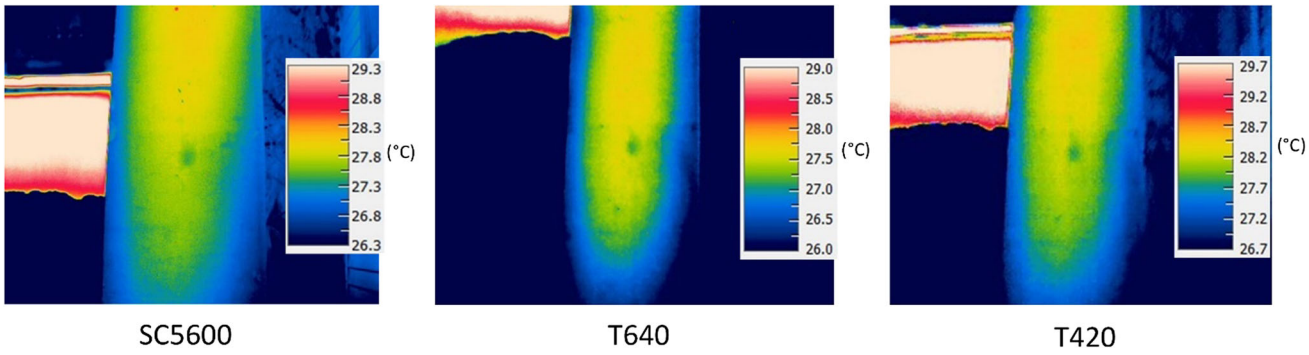

Fig. 31 Raw IR images taken by each camera

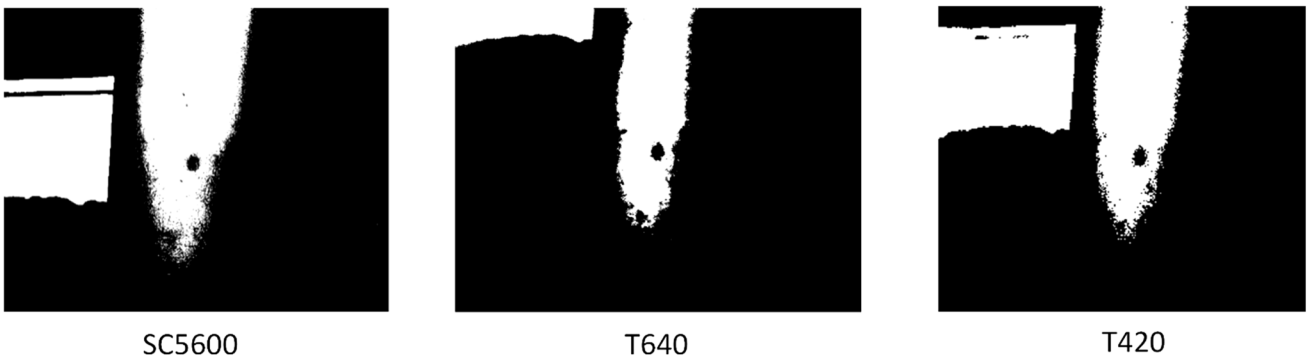

Fig. 32 Processed IR images taken by each camera

[24]. As displayed in Fig. 30, after the delamination was found by IRT, that location was hammered and a delaminated spot was revealed. In this study, the IR data collected by three cameras before hammering were used for the application of the data processing method. Figure 31 shows raw IR images in which the temperature spans were set up to recognize the delaminated area easily at the middle of the structure under the temperature range setting of 3.0 K. These IR images were taken at the distance of approximately 4.0 m from the structure with no angle at nighttime, around 9 P.M. Therefore, the delaminated area should be displayed as a cooler temperature than the surroundings, and every camera indicated the cooler spot at the middle of the structure, even though the parts on the edge of the structure also show cooler temperature values due to the boundary condition.

Figure 32 depicts processed IR images by the same way as described in Sect. 5.1. Since temperatures of the delaminated area and the surroundings were already known, the processing methodology was easily applied for this IR data. As can be seen in Fig. 32, each IR data clearly indicates a delaminated area at the middle of the structure, even though these processed images also depict misdetection due to the boundary condition as in the raw IR images. However, the area where it is not affected by the boundary condition displays very clear damage detection on the processed images. Therefore, this methodology has a potential to improve delamination detection by IRT for concrete structures, especially huge areas of concrete surfaces such as concrete bridge decks, namely, most of the area is not affected by the boundary condition.

However, there are two challenges to improve the methodology. Firstly, how to obtain the information of temperature difference between sound and delaminated areas becomes a challenge for this methodology. Since temperatures of the delaminated area and the surroundings at the structure were already known, the processing methodology was easily applied for those IR data. However, for unknown defects, it is important to explore the temperature difference between sound and delaminated portions. Finite Element Method (FEM) might be one of the ways to simulate the temperatures as discussed in [24, 25]. Since even IR cameras provide different temperature readings depending on camera specifications and the photography angle, it is impossible to obtain both T(del.) and T(sound) from FEM analysis. Furthermore, since temperature differences between the sound and delaminated parts were very small, less than 0.5 °C in this experiment, even 1 or 2 °C of slight error leads different results in this method. However, finite element modeling can simulate the

temperature differences accurately [24, 25], and the temperature differences are almost identical despite camera specifications and the photography angle. Therefore, if T(del.) or T(sound) can be obtained, $F(x, y)$ can also be gained based on FEM analysis; consequently, this method is applicable. In terms of the reference temperature of the sound or delaminated point, the temperature of the sound area should be chosen for the threshold value. Since the majority of concrete surfaces are sound and would have homogeneous temperature, it is much easier to obtain T(sound) from IR images. Moreover, the location of the delaminated area is usually unknown and this method is trying to detect the delaminated part. To investigate the practicability of this method for real concrete structures, further experiments under passive IR condition are needed.

Second, how to remove the effect of boundary condition around the edge part of the structures is another challenge. Regarding the effect of boundary condition, the effect of data collection time should also be considered. As Watase et al. [8] argued that there is an ideal time for IRT, there might be a different effect in terms of boundary condition depending on the time. Therefore, favorable time window for IRT should be explored.

7 Conclusions

By considering different camera technologies, IR image collection with different angles and using an objective data analysis method for laboratory and field studies, the following conclusions can be drawn from the findings.

1. Three different types of IR cameras were compared to examine how camera specifications affect the results of IRT for subsurface delamination detection of concrete structures. Three concrete plates with different thicknesses were used to simulate artificial delamination, and they were attached onto a wooden board, which was equipped with an electric heating mat to heat up the board and test specimens. Infrared images were taken from a distance of 5.0 m by the three different IR cameras at the same time with angles of 0°, 30° and 45° (where 0° is perpendicular). This comparative study leads following conclusions:
   (a) In the comparison of IR readings, it is found that when IR images are taken from an angle perpendicular from the objects, IRT is less sensitive than when they are taken from a certain angle regarding temperature reading of different types of IR cameras.
   (b) Even though different IR cameras capture different temperatures from the concrete surface when they are utilized at a certain angle, they have a potential to detect delaminated areas under a given condition in spite of camera specifications.
   (c) Regarding the comparison of IR images, no big difference can be recognized from IR images taken at this laboratory test. However, SC5600 depicts the indications most clearly among these three cameras in any cases and times, and SC5600 and T640 yielded color contrast between the delaminated and sound areas faster than T420. These results indicate that the thermal sensitivity/accuracy and resolution might affect IRT results regarding the visibility of damage indication.
2. Since the temperature difference between the sound and delaminated parts was very small, less than 0.5 °C in this experiment, the color contrast of IR images became unclear, and it became difficult and subjective to judge IR images. Therefore, a more objective data processing method was developed using MATLAB in this study. Through the comparison of processed images, the followings were also found;
   (a) Only T420 shows lower performance than the other two cameras in terms of delamination detection for IRT. Although SC5600 performs more accurately than T640 since it displays closer shapes of delamination in each case, both cameras successfully depict delaminations at the middle areas of all test specimens after a certain time from the beginning of heating at this laboratory test. From the results, it is certain that the pixel resolution of the IR camera affects the performance of IRT, 320 × 240 pixels for 5.0 m distance photography in this case.
   (b) Thermal sensitivity or accuracy also might affect IRT results since SC5600 shows better performance than T640.
3. In this study, the developed data processing methodology made it much easier to detect delamination than raw IR images. Since this experiment was conducted by active IRT condition, the study tried to apply this methodology to a real concrete structure under passive IRT condition to investigate how it would work. In the application to the structure, it was revealed that:
   (a) Each IR data clearly indicates delaminated area at the middle of the structure, even though it depicts misdetection due to the boundary condition in the same way as raw IR images.
   (b) However, the area where it is not affected by the boundary condition displays very clear damage detection on the processed images. Therefore,

this methodology has a potential to improve delamination detection by IRT for concrete structures, especially huge areas of concrete surfaces such as concrete bridge decks, namely, most of the area that is not affected by the boundary condition.

4. There are two challenges to improve the methodology:
   (a) How to obtain the information of temperature difference between sound and delaminated areas becomes a challenge for this methodology. FEM is the promising way to obtain the temperature difference for processing IR data.
   (b) How to remove the effect of boundary condition around the edge part of the structures is another challenge. Regarding the effect of boundary condition, the effect of data collection time should also be considered. Since there is an ideal time for IRT, there might be a different effect in terms of boundary condition depending on the time. Therefore, favorable time window for IRT should be explored.

Acknowledgments The authors would like to express their sincere gratitude to Dr. Koji Mitani, Mr. Masato Matsumoto, Mr. Shinji Nagayasu and Mr. Kyle Ruske of NEXCO-West USA for their feedback and support throughout the studies presented in this manuscript. Without their contributions, this project would not have been realized. The authors also wish to acknowledge the financial support of Tübitak (The Scientific and Technological Research Council of Turkey) for supporting the 2nd author while he was a visiting scholar at UCF.

References

1. NEXCO-West (2014) Manual for maintenance of road structures. Company maintenance manual, Osaka, Japan **(in Japanese)**
2. ASTM (2014) Standard test method for detecting delaminations in bridge decks using infrared thermography, ASTM Designation D4788-03 ed. ASTM International, West Conshohocken. doi:10.1520/D4788-03R13.2
3. Washer GA, Fenwick RG, Bolleni NK (2009) Development of hand-held thermographic inspection technologies. Final Report Submitted to Missouri Department of Transportation, Report No. OR10-007
4. Washer G, Fenwick R, Bolleni N (2010) Effects of solar loading on infrared imaging of subsurface features in concrete. J Bridge Eng 15:384–390. doi:10.1061/(ASCE)BE.1943-5592.0000117
5. Gucunski N, Nazarian S, Yuan D, Kutrubes D (2013) Nondestructive testing to identify concrete bridge deck deterioration. Transportation Research Board, SHRP 2 Report S2-R06A-RR-1, Washington, D.C., USA
6. Yehia S, Abudayyeh O, Nabulsi S, Abdelqader I (2007) Detection of common defects in concrete bridge decks using nondestructive evaluation techniques. J Bridge Eng 12:215–225. doi:10.1061/(ASCE)1084-0702(2007)12:2(215)
7. Kee S-H, Oh T, Popovics JS et al (2012) Nondestructive bridge deck testing with air-coupled impact-echo and infrared thermography. J Bridge Eng 17:928–939. doi:10.1061/(ASCE)BE.1943-5592.0000350
8. Watase A, Birgul R, Hiasa S et al (2015) Practical identification of favorable time windows for infrared thermography for concrete bridge evaluation. Constr Build Mater 101:1016–1030. doi:10.1016/j.conbuildmat.2015.10.156
9. Maierhofer C, Brink A, Ro M, Wiggenhauser H (2005) Quantitative impulse-thermography as non-destructive testing method in civil engineering—experimental results and numerical simulations. Constr Build Mater 19:731–737. doi:10.1016/j.conbuildmat.2005.06.002
10. Cheng C-C, Cheng T, Chiang C (2008) Defect detection of concrete structures using both infrared thermography and elastic waves. Autom Constr 18:87–92. doi:10.1016/j.autcon.2008.05.004
11. Abdel-qader I, Yohali S, Abudayyeh O, Yehia S (2008) Segmentation of thermal images for non-destructive evaluation of bridge decks. NDT & E Int 41:395–405. doi:10.1016/j.ndteint.2007.12.003
12. Farrag S, Yehia S, Qaddoumi N (2015) Investigation of mix-variation effect on defect-detection ability using infrared thermography as a nondestructive evaluation technique. J Bridge Eng 21:04015055. doi:10.1061/(ASCE)BE.1943-5592.0000779
13. Hiasa S, Catbas FN, Matsumoto M, Mitani K (2015) Testing of dynamic infrared thermography application for subsurface damage detection in concrete structures. In: International symposium non-destructive testing in civil engineering (NDTCE 2015). Bundesanstalt für Materialforschung und –prüfung (BAM), Berlin
14. Hiasa S, Catbas FN, Matsumoto M, Mitani K (2016) Feasibility of infrared thermography for bridge deck inspection without lane closure, and the uncertainties—preliminary report-TRB 95th Annu. Meet
15. Nishikawa T, Hirano A, Kamada E (2000) Experimental study on thermography method for external wall removement finished with ceramic tile. Archit Inst Jpn 529:29–35
16. Nakamura S, Takaya S, Maeda Y et al (2013) Spalling time prediction by using infrared thermography. J Jpn Soc Civ Eng Ser E2 Mater Concr Struct 69:450–461
17. Hashimoto K, Akashi Y (2010) Points to consider for photography by infrared cameras with different wavelength detection region. In: 65th JSCE Annu. Meet. Japan Society of Civil Engineers (JSCE), Sapporo, Japan, pp VI–160
18. Oh T, Kee S, Arndt RW et al (2013) Comparison of NDT methods for assessment of a concrete bridge deck. J Eng Mech 139:305–314. doi:10.1061/(ASCE)EM.1943-7889.0000441
19. Washer G, Fenwick R, Nelson S, Rumbayan R (2013) Guidelines for thermographic inspection of concrete bridge components in shaded conditions. Trans Res Rec J Trans Res Board 2360:13–20. doi:10.3141/2360-02
20. Chase S, Adu-Gyamfi Y, Tunuguntla P (2015) Bridge deck subsurface defect detection using time-lapse thermography. TRB 94th Annu. Meet
21. FLIR (2013) The ultimate infrared handbook for R&D professionals. FLIR AB. (T559243{en-SV}_A). http://www.flirmedia.com/MMC/THG/Brochures/T559243/T559243_EN.pdf
22. Holst GC (2000) Common sense approach to thermal imaging. JCD Publishing, Winter Park
23. Tashan J, Al-mahaidi R, Mamkak A (2015) Defect size measurement and far distance infrared detection in CFRP-concrete and CFRP-steel systems. Aust J Struct Eng. doi:10.1080/13287982.2015.1116177
24. Catbas FN, Hiasa S, Khuc T et al. (2015) Development, implementation and evaluation of image-based technologies for civil infrastructure systems. Report submitted to West Nippon Expressway Company limited (NEXCO-West), Osaka, Japan
25. Rumbayan R, Washer GA (2014) Modeling of environmental effects on thermal detection of subsurface damage in concrete. Res Nondestruct Eval 25:235–252. doi:10.1080/09349847.2014.933993